Journal of Applied Physics

AIP Publishing

Bulk modulus and thermal expansion of rare-earth tetraborides RB_4 (R=Gd, Tb, Dy, Ho and Tm) via in situ X-ray diffraction

Hitoshi Yusa[*,1] and Fumitoshi Iga*[2]

[1]Research Center for Materials Nanoarchitectonics, National Institute for Materials Science, 1-1 Namiki, Tsukuba, Ibaraki 305-0044, Japan

[2]Institute of Quantum Beam Science, Ibaraki University, 2-1-1 Bunkyo, Mito, Ibaraki 310-8512, Japan

*Corresponding author E-mail: yusa.hitoshi@nims.go.jp

Abstract

X-ray diffraction experiments were conducted on the rare-earth tetraborides RB_4 (R=Gd, Tb, Dy, Ho and Tm) under high pressure at room temperature and low temperature at atmospheric pressure to investigate their structural and lattice behavior, and thus determine their bulk moduli and thermal expansion coefficients. The bulk modulus values ranged from 175 to 180 GPa for all rare earths. These values lie between those of RB_6 and RB_{12} structures and do not exhibit a simple correlation with boron concentration, but rather correlate with the R–B distance in the coordination polyhedron. RB_4, which features a tetragonal crystal structure with a Shastry–Sutherland lattice, shows anisotropy where the *c*-axis is more compressible than the *a*-axis. Additionally, lattice contraction due to temperature changes exhibits similar anisotropy. Considering the *a*/*c* anisotropy per unit volume, the present result indicates that the thermal contraction effect is greater than the compression effect.

I. INTRODUCTION

Boron, with only three valence electrons and a tendency for electron deficiency in conventional three-dimensional bonding, overcomes this by forming strongly covalent-bonded boron clusters that exhibit high melting points, hardness, and low compressibility.[1] Furthermore, boron readily bonds with rare-earth elements, whose electrons stabilize the boron cluster and create a unique coordination cage around the rare-earth element. From a crystallographic perspective, rare-earth polyborides exhibit two key features: a boron cluster and framework with strong covalent bonds within the crystal structure, and a highly coordinated structure centered on the coordination cage. Specifically, in RB_4 and RB_6, they form six-boron octahedron clusters, whereas in RB_{12} they form dodecahedron clusters (cuboctahedron), as shown in Fig. 1(a)–(c). By contrast, focusing on the coordination cage, as shown in Fig. 1(d)–(f), RB_4 features a double-bicapped heptagonal prism with a coordination number of 18, RB_6 presents a truncated cube with a coordination number of 24, and RB_{12} also has a coordination number of 24 but forms a truncated octahedron. Among these borides, only RB_4 exhibits a tetragonal crystal structure. Particularly, the network of rare-earth atoms in the (001) plane of RB_4, as depicted in Fig. 1(g), features a unique topology equivalent to the Shastry–Sutherland lattice (SSL),[2] known for its magnetic frustration, which has been widely reported to impart diverse magnetic properties to various RB_4 compounds.[3-9] Therefore, it is fundamentally important to examine the anisotropy of these lattice contractions caused by changes in pressure and temperature.

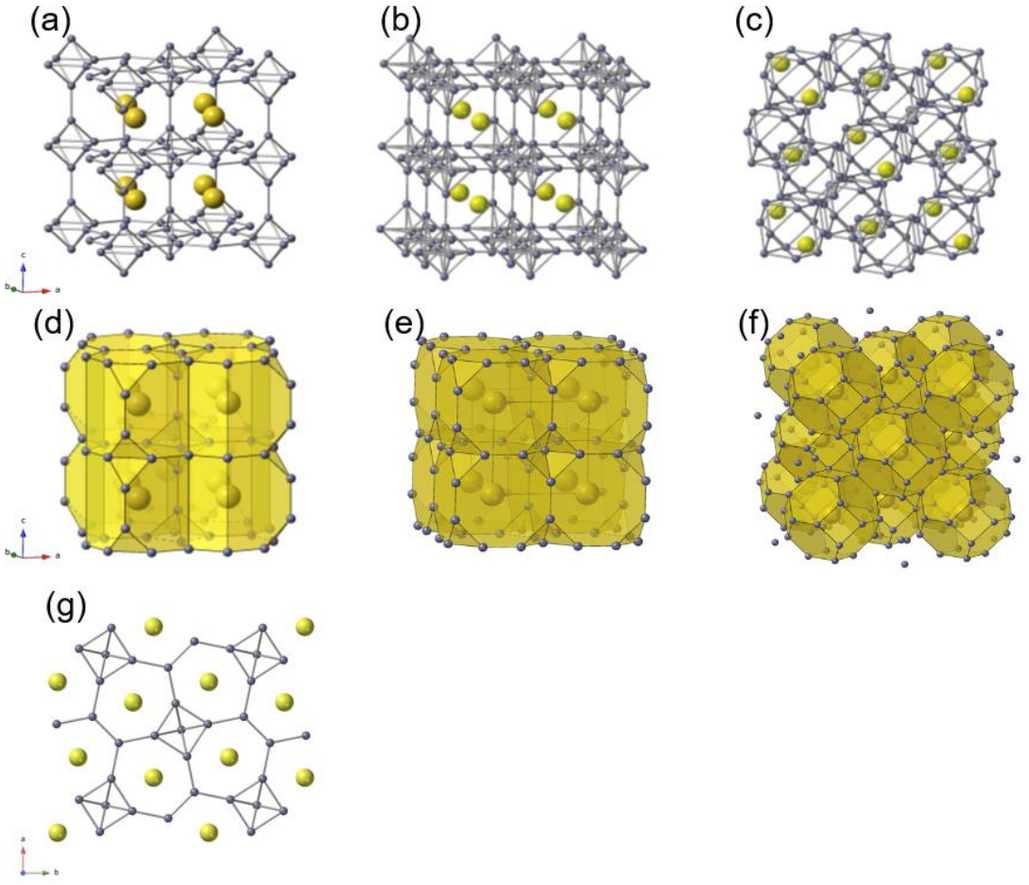

Figure 1 : Comparison of crystal structures of various borides (RB_4, RB_6, and RB_{12}). (a), (b), and (c) highlight the boron clusters in the structure, while figures (d), (e), and (f) are illustrated based on the coordination cage structure. (g) depicts the network of SSL in the (001) plane of RB_4.

The aim of this study was to precisely determine the bulk modulus, which represents the hard characteristics of these polyborides, specifically for RB_4. Furthermore, we sought to compare the bulk modulus with that of other polyborides, such as RB_6 and RB_{12}, to clarify the correlation between structure and bulk modulus. We focused on rare-earth tetraborides RB_4 (R=Gd, Tb, Dy, Ho and Tm). These RB_4 exhibited unique properties as SSL magnetic materials. All of them have large magnetic moments and were found to exhibit many anisotropic magnetic order phases.[3,10-13] Among these, HoB_4 is the only compound for which an experimentally determined bulk modulus has been reported.[14] However, there are no reported measurements of the elastic properties of other RB_4 borides. Even when considering theoretical calculations for RB_4, the only available results from first-principles calculations are for LuB_4, CeB_4 and LaB_4.[15-18] In this study,

we conducted in situ X-ray diffraction experiments under high pressure for the five borides of the heavy rare-earth elements mentioned above and systematically derived their bulk moduli.

There are also limited studies on the temperature dependence of the lattice parameter in RB_4. Previous studies have shown significant discrepancies for HoB_4,[14,19] and reports for LaB_4, SmB_4, GdB_4, TbB_4, DyB_4, and TmB_4 are available only from the same research group.[18-22] In this study, we revisited previous research by precisely determining the lattice parameters of these RB_4 compounds using synchrotron X-ray diffraction and deriving their thermal expansion coefficients. Additionally, we compared the anisotropy of lattice contraction at low temperatures with that caused by pressure effects.

II. EXPERIMENTAL

Tetraboride samples (RB_4: R = Gd, Tb, Dy, Ho, and Tm) were prepared as follows. Each high-purity rare-earth sesquioxide reagent (Gd_2O_3, Tb_2O_3, Dy_2O_3, Ho_2O_3, and Tm_2O_3; 99.99 % purity: Rare Metallic Co., Ltd, Japan.) and boron powder (99% purity: Kojundo Chemical Laboratory Co., Ltd., Japan) were mixed using an automatic mortar for 30 minutes and then compacted using a cold isostatic pressing device (Nikkiso Co., Ltd., Japan) to a rod shape under 250 MPa at ambient temperature. As a first step, the compacted rod-shaped samples were heated using a radio-frequency induction furnace under vacuum. The reaction proceeded at 1700 ºC as follows:

$$R_2O_3 + 11B \rightarrow 2RB_4 + 3BO \uparrow$$

As a second step, these sintered rods were grown into single crystals under an argon flow by the floating-zone method using an image furnace equipped with four xenon lamps.[23] These purified samples were then finely powdered for X-ray diffraction.

In situ X-ray powder diffraction experiments under high pressure were conducted at BL18C and AR-NE1 at Photon Factory (KEK) using angle-dispersive monochromatic X-ray with wavelengths of 0.621787 and 0.417051 Å, respectively. Compression experiments were performed using a diamond anvil cell (DAC; Syntek Co., Ltd., Japan) with diamond culet diameters of 0.4–0.6 mm at room temperature. Specifically, at BL18C, a Boehler-Almax design diamond anvil was attached to a DAC with a large aperture angle, allowing the collection of diffraction lines on the high-angle side even with long-wavelength X-rays. The sample was mixed with gold powder and placed in a 120-μm-diameter hole in a stainless-steel gasket that had been indented to a

thickness of approximately 60 μm. The hole was filled with an alcohol mixture (methanol: ethanol: water = 16:3:1 by volume) together with a ruby pressure marker. The X-rays were collimated to a diameter of 50 μm and irradiated onto the sample in the DAC. The experiments were carried out under hydrostatic pressure up to 10 GPa. The pressure was determined from the diffraction lines of the gold powder mixed with the sample using an equation of state.[24] Diffraction X-rays were detected using either an imaging plate (FUJI Film BAS IP Co., Ltd., Japan) or a complementary metal–oxide semiconductor (CMOS) flat panel detector (Teledyne Vison Solutions Rad-icon 2022, USA). All XRD profiles were converted to intensity–2θ data using IPAnayzer software.[25] The lattice parameters were refined by profile fitting with PDIndexer software[25] and the LeBail method of the GSAS.[26]

The X-ray diffraction experiments at low temperature and room temperature under ambient pressure were conducted at BL2S1 of the Aichi Synchrotron Radiation Facility (AichiSR). Monochromatic X-rays (λ = 0.722782 Å) collimated to a size of 100 μm were irradiated onto samples fixed in polyimide capillaries. Diffracted X-rays were detected using a hybrid pixel array detector (PILATUS 1M, Dectris, Switzerland). The X-ray diffraction patterns of the initial samples are shown in Fig. S1(a)–(e). The lattice parameters summarized in Table 1 are in good agreement with the reported values. Cooling experiments were performed by blowing nitrogen gas from a refrigerator onto the capillary sample. The temperature was calibrated using diffraction lines from a small amount of gold powder coated on the sample.[27] All lattice parameters were refined using the LeBail method of the GSAS.[26]

III. RESULTS AND DISCUSSION

Figure S2(a)–(e) shows the X-ray diffraction patterns of each RB_4 compound with increasing pressure. Within the measured pressure range, no structural phase transitions were observed at room temperature under high pressure for any of the RB_4 compounds. As shown in Fig. S2, peak broadening due to increased pressure was not observed, indicating that hydrostatic pressure was maintained, which supports the small error in the lattice constants shown in Table SI. The volume of each RB_4 compound in Fig. 2(a)–(e) monotonically decreased with pressure. All lattice parameters obtained under high pressure are provided in Table SI(a)–(e). The volume data were fitted using the Birch–Murnaghan equation of state to determine the bulk modulus (B_0) with the pressure derivative (B_0') fixed at 4. The bulk and linear moduli are presented in Table I. As mentioned above, the bulk modulus has only been measured experimentally for HoB_4. This value (195(5) GPa)[28] is higher than that measured in the present study. Furthermore,

considering the scattering in their P–V data[28] and the standard deviation being 10 times greater than the present value, their value is not highly accurate. Bulk moduli have been independently calculated for the lanthanide tetraborides LuB_4 (183.5 GPa) and HoB_4 (198.2 or 188.4 GPa). These values are consistent with those of the present study. However, all previous studies were conducted individually. In the present study, multiple compounds were measured, allowing for a systematic comparison.

TABLE I: Lattice parameters and bulk moduli (B_0) and linear moduli (M_0) of RB_4

Compounds	a(Å)	M_{0a}(GPa)	c(Å)	M_{0c}(GPa)	V (Å^3)	B_0(GPa)
GdB_4	7.14487 (3)	555(1)	4.04759 (3)	490(2)	206.626 (2)	177.2 (4)
TbB_4	7.11939 (3)	553(2)	4.02881 (3)	485(2)	204.203 (2)	176.1 (3)
DyB_4	7.10134 (3)	550(2)	4.01644 (3)	480(2)	202.545 (1)	175.0 (3)
HoB_4	7.08691 (2)	563(1)	4.00609 (2)	480(3)	201.203 (1)	177.7 (4)
TmB_4	7.05688 (3)	571(2)	3.98605 (3)	473(1)	198.504 (2)	178.4 (4)

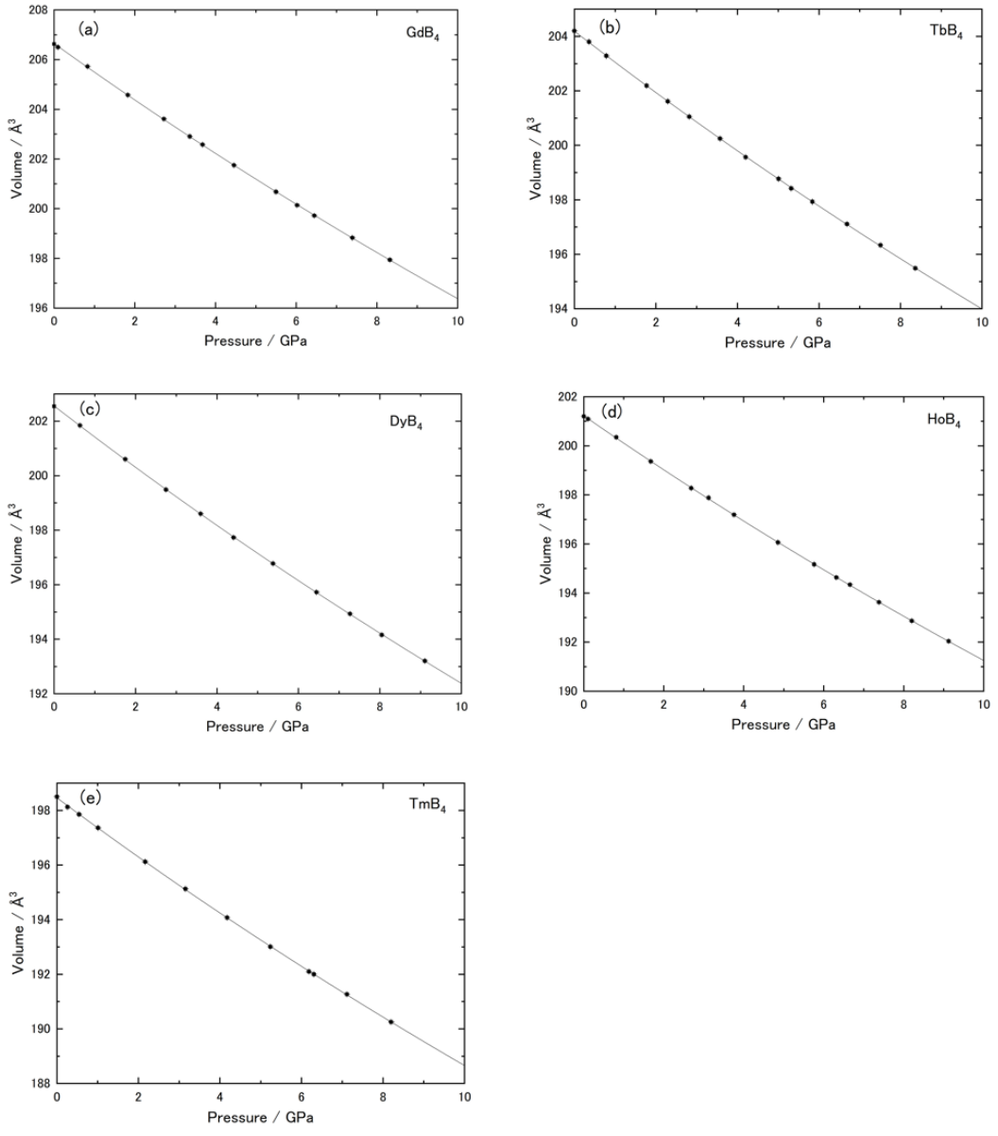

Figure 2 : *P-V* data and compression curve for RB_4. (a) GdB_4, (b) TbB_4, (c) DyB_4, (d) HoB_4, and (e) TmB_4. Phase transitions have not appeared in all compounds. As shown in Table SI, the error is so small that it is almost within a symbol.

The bulk moduli of the different compounds in the present study were almost identical, ranging from 175 to 180 GPa, regardless of the lanthanide atomic number. Generally, the bulk modulus of a given structure is inversely proportional to the volume at atmospheric pressure, with the rule that B_0V_0 is a constant having been empirically established.[29] As depicted in Fig. 3(a), the V_0 of the present RB_4 compounds decreased with increasing atomic number, following the lanthanide shrinkage effect. Figure 3(b) re-evaluates the relationship between volume and bulk modulus, as proposed by Anderson

and Anderson (1970)[29]. However, no such correlation was found in RB_4 measured in this study. As an explanation, we focused on the lattice constants and linear modulus of each axis. A plot of their correlation is shown in Fig. S3. According to this, the linear modulus of the *a*-axis decreases with an increase in the lattice constant, while that of the *c*-axis increases. In other words, despite the change in volume, the bulk modulus remains almost constant due to the behavior of the *c*-axis. This may be caused by the anisotropic distribution of *f*-electrons in the *c*-axis direction.

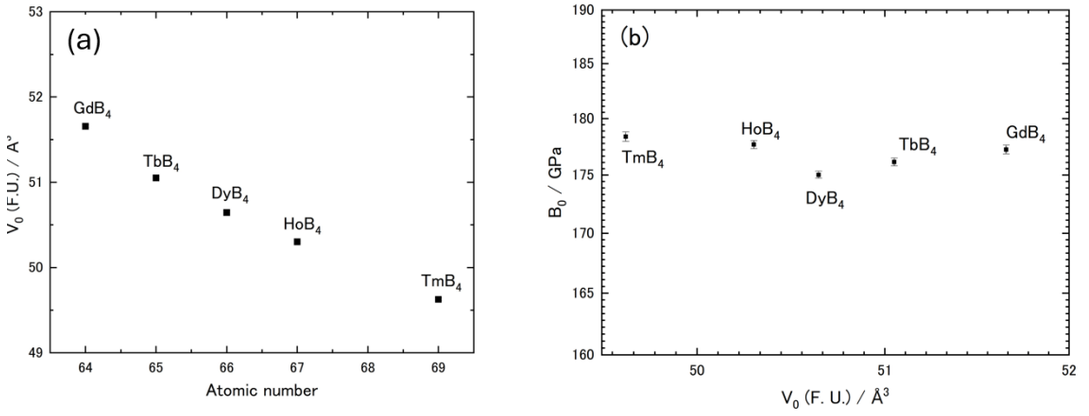

Figure 3 : (a) Volume per formula unit (V_0) versus atomic number for GdB_4, TbB_4, DyB_4, HoB_4, and TmB_4. (b) Bulk moduli (B_0) versus volume per formula unit (V_0) plotted on a double logarithmic axis.

The pressure dependence of the *a*- and *c*-axes and their ratio (*a*/*c*) of each compound in RB_4 are plotted in Fig. 4(a)–(c), respectively. The linear elastic modulus for each axis, as presented in Table I, indicates that the *c*-axis is about 12%–17% more compressible than the *a*-axis. As demonstrated by the intercept in Fig. 4(c), the ratio (*a*/*c*) decreased with increasing atomic number, suggesting that the contraction of the *c*-axis is more strongly correlated with number of *f*-electrons of the lanthanoid atoms. An increase in pressure caused further contraction of the *c*-axis, possibly indicating the anisotropic distribution of *f*-electrons in the direction of the *c*-axis. Examining the crystal structure, particularly in the case of GdB_4, the distance between lanthanide atoms revealed that the Gd–Gd distance along the *c*-axis is about 10% longer than the Gd–Gd distance in the *c*-plane. This suggests that atoms are more easily compressed along the *c*-axis. From a crystallographic perspective, this anisotropic behavior is not observed in cubic borides,

such as RB_6 and RB_{12}, and can be considered unique to RB_4 owing to its SSL.

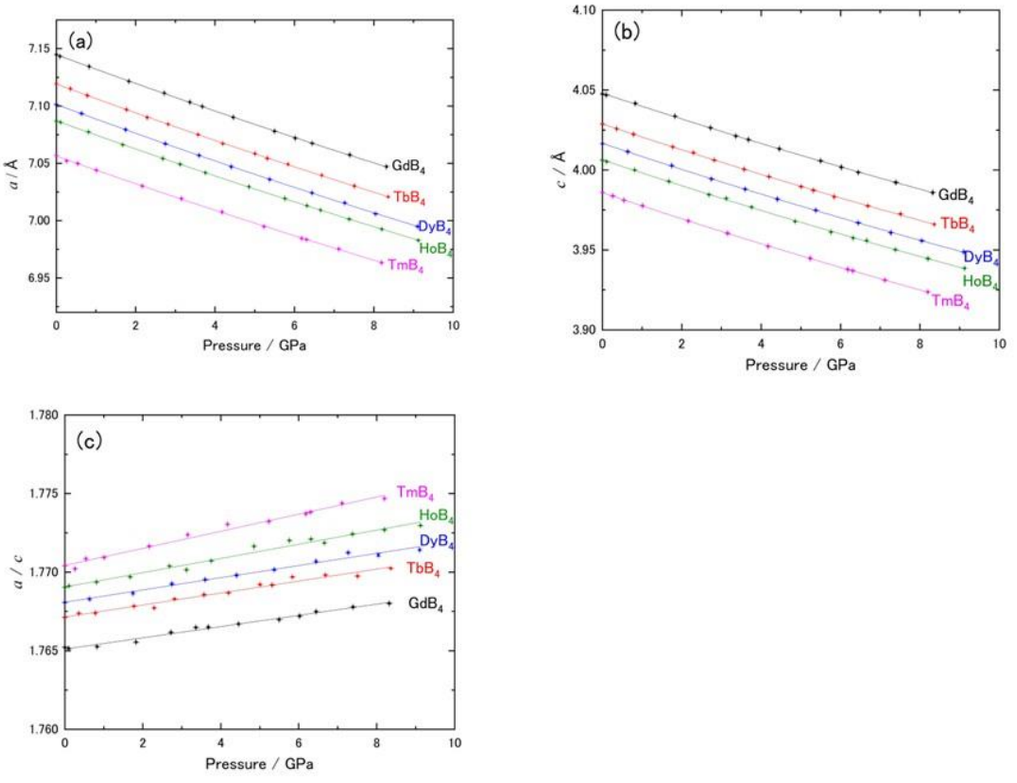

Figure 4 : Pressure dependence of the *a*-axis (a), *c*-axis (b) and their ratio (*a*/*c*) (c) for each compound in RB_4. As shown in the linear modulus of elasticity in Table I, the *c*-axis is more compressible than the *a*-axis. Therefore, *a*/*c* increases with pressure.

We now compare the bulk modulus of RB_6 and RB_{12}. In our previous work,[30] we successfully synthesized PrB_{12} and CeB_{12}, and measured the bulk moduli of PrB_6 and CeB_6, which showed values of 206(1)–208(1) GPa and 165(1)–168(1) GPa, respectively. Additionally, our preliminary measurements of the bulk modulus of NdB_{12} and NdB_6 showed values of 207(1) GPa and 168(1) GPa, respectively, which are close to these values, suggesting that the bulk modulus may be nearly constant regardless of the lanthanide atom. Therefore, we can conclude that the RB_4 structure has an intermediate bulk modulus between RB_6 and RB_{12} and that there is no simple correlation with the boron concentration. Assuming that the bulk moduli of GdB_6 and GdB_{12} are comparable to those of RB_6 and RB_{12} shown above, we discuss the correlation between interatomic distances and bulk moduli across these structures. In a previous paper, we demonstrated that the R–B distances in the distinct 24-coordinated cages of RB_6 and RB_{12} are 7.2%–

7.8% shorter in RB_{12}, contributing to the difference in bulk modulus. This difference is nearly identical for GdB_6 and GdB_{12}, which have average R–B distances of 3.02 and 2.79 Å, respectively. RB_4 consists of an 18-coordinated polyhedron, and the average R–B distance for GdB_4 is 2.83 Å, which is about 6% shorter than that of GdB_6 with its 24-coordinated polyhedron. This may be a reason why RB_4 has a larger bulk modulus than RB_6.

Another method for verifying the anisotropy of the axial ratio during volume change is to measure the lattice constant at low temperatures. The change in each lattice constant (volume, *a*-, and *c*-axis) and the axial ratio (*a*/*c*) are shown in Fig. 5(a)–(d). As depicted in Fig. 5(d), anisotropic shrinkage of the lattice was observed at low temperatures, similar to that observed under high pressure.

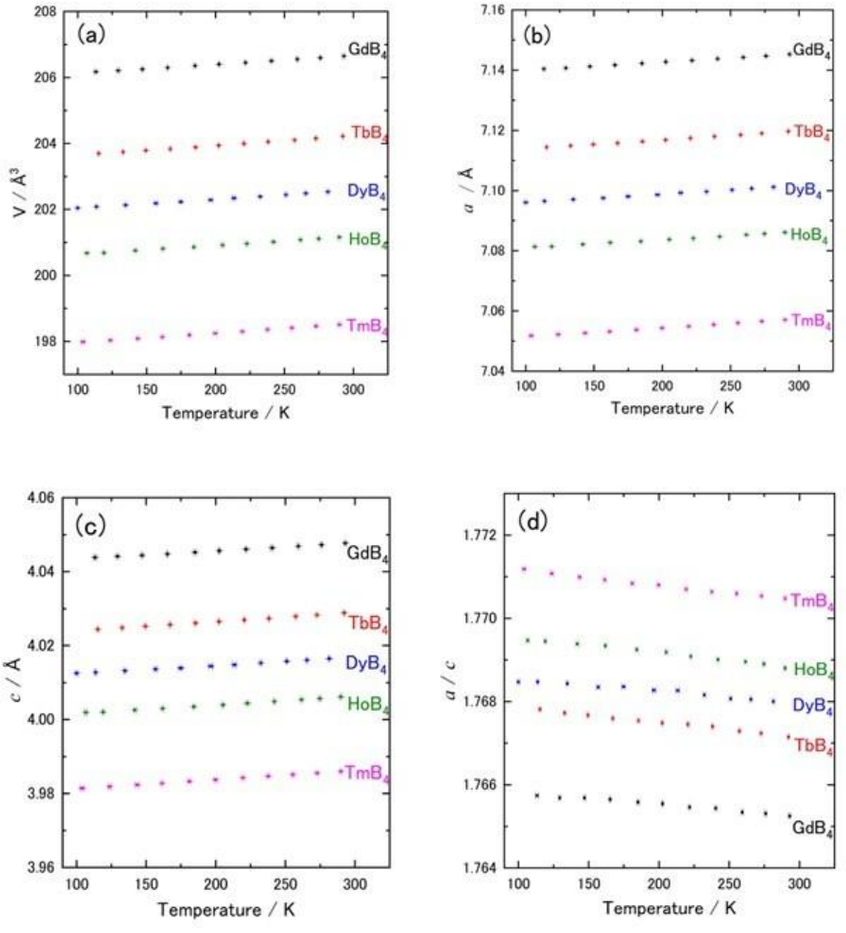

Figure 5 : Temperature dependence of the *a*-axis (a), *c*-axis (b) and volume (c), and their (*a*/*c*) (d) for each compound in RB_4. Note the increase in anisotropy, indicated by *a*/*c*, due

to cooling.

Previous research has reported that the HoB_4 crystal splits along the *a*-axis owing to a change in symmetry at temperatures below room temperature; [28] however, we did not observe this behavior in our measurements. Novikov et al.[22] reported lattice parameter changes in six borides from GdB_4 to LuB_4, including HoB_4, through X-ray diffraction experiments at low temperatures, but did not report structural changes in HoB_4. Comparison of their results with the present measurements for other RB_4 compounds shows a generally similar trend.

We calculated the coefficient of thermal expansion from the lattice constants obtained in the present study. The thermal expansion coefficient at temperature, *T*, is defined by Equation (1):

$$\alpha(T) = \frac{1}{V(T)}\left(\frac{\partial V}{\partial T}\right)_P. \quad (1)$$

The volume at the standard temperature of 298 K is given by Equation (2). In this case, the thermal expansion coefficient at a given temperature *T* is set as α(*T*) in the linear form of Equation (3):

$$V_0^T = V_0^{298} exp \int_{298}^{T} \alpha\,(T) dT; \quad (2)$$

$$\alpha(T) = \alpha_0 + \alpha_1 T. \quad (3)$$

Using the temperature variation of the lattice constant, the coefficients α_0 and α_1 were determined using the least-squares method. The thermal expansion coefficients are summarized in Table II.

TABLE II: Thermal expansion coefficients of volume (α_v), a (α_a) and c (α_c)

Compounds	$\alpha_v(T) = \alpha_{v0} + \alpha_{v1} T$ (K^{-1})		$\alpha_a(T) = \alpha_{a0} + \alpha_{a1} T$ (K^{-1})		$\alpha_c(T) = \alpha_{c0} + \alpha_{c1} T$ (K^{-1})	
	$\alpha_{v0} \times 10^5$	$\alpha_{v1} \times 10^8$	$\alpha_{a0} \times 10^5$	$\alpha_{a1} \times 10^8$	$\alpha_{c0} \times 10^5$	$\alpha_{c1} \times 10^8$
GdB_4	1.04(7)	1.20(34)	0.34(3)	0.19(14)	0.37(3)	0.82(17)
TbB_4	1.07(5)	1.86(26)	0.30(3)	0.56(16)	0.47(3)	0.74(13)
DyB_4	0.94(7)	2.08(35)	0.31(3)	0.42(18)	0.30(3)	1.27(18)
HoB_4	0.92(12)	2.04(59)	0.28(5)	0.48(22)	0.34(4)	1.20(22)
TmB_4	1.17(6)	1.39(30)	0.29(2)	0.64(12)	0.60(2)	0.11(11)

Figure 6 presents a graphical representation of the thermal expansion coefficients as a function of temperature. The volume thermal expansion coefficients of these borides generally ranged from 1.1 to 1.6×10^{-5} K^{-1}, although there was some temperature dependence, as shown in Fig. 6(a). The linear thermal expansions of the *a*- and *c*-axes are indicated in Fig. 6(b) and (c). In previous studies, electromagnetic phase transitions have been observed in GdB_4, TbB_4, DyB_4, and HoB_4 at temperatures below 50 K,[19-22,31] and lattice parameter changes reflecting these transitions have been reported based on X-ray diffraction experiments.[19] Because our measurements were conducted above 90 K, the information on lattice contraction is less sensitive to these effects. Taking this into account, we compared the thermal expansion coefficients of GdB_4 and TbB_4 with those reported previously.[20,22] For TbB_4, the thermal expansion coefficients along the *a*- and *c*-axes were reported to be 2.2 to 5.2×10^{-6} and 4.4 to 6.8×10^{-6} K^{-1}, respectively; for GdB_4, they were 1.7 to 4.8×10^{-6} and 3.1 to 7.0×10^{-6} K^{-1}, respectively. These values are in good

agreement with our data shown in Fig. 6(b) and (c).

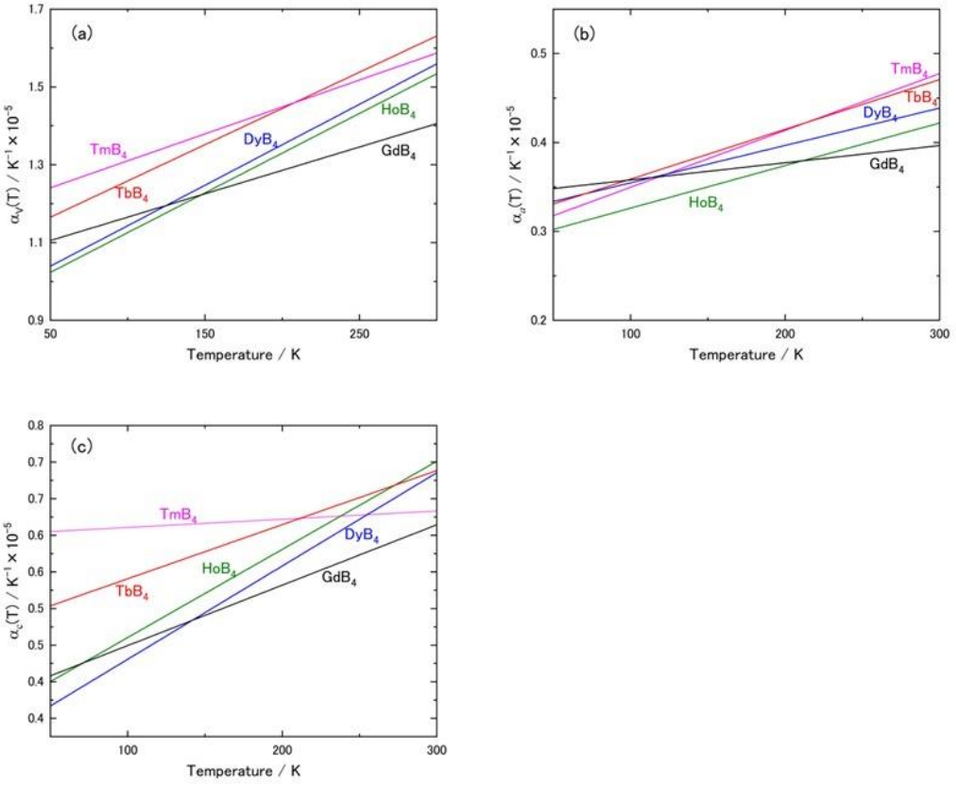

Figure 6 : Thermal expansion coefficients of each RB_4 as a function of temperature. (a) Volume thermal expansion, (b) linear thermal expansion of *a* axis, and (c) *c* axis.

We now compare the linear thermal expansion coefficients with those of RB_6 measured in previous studies. For instance, the values reported by Shirota et al.[32] for GdB_6, TbB_6, and DyB_6 in the temperature range of 90–300 K were 5.4 to 6.4 × 10^{-6}, 3.5 to 6.0 × 10^{-6}, and 5.0 to 6.2 × 10^{-6} K^{-1}, respectively. These values are similar to those corresponding to the *c*-axis of RB_4 in this study. Conversely, this suggests that the values for the *a*-axis of RB_4 are relatively small, which may be related to the fact that R ions in the *c*-plane form a Shastry–Sutherland-type geometric lattice.

Finally, we compare the effects of temperature and pressure on lattice anisotropy. By plotting the change in lattice anisotropy $\Delta(a/c)$ per unit volume change in Figure 7, it can be seen from the slope of the linear regression that the volume contraction due to temperature change is approximately 3 to 3.5 times larger than that due to compression. This suggests that even at temperatures up to 90 K, some magnetic interaction originating from the SSL characteristic of the *c*-plane may be involved. However, to accurately verify

this behavior, magnetic measurement studies under low-temperature and high-pressure conditions may be necessary in the future.

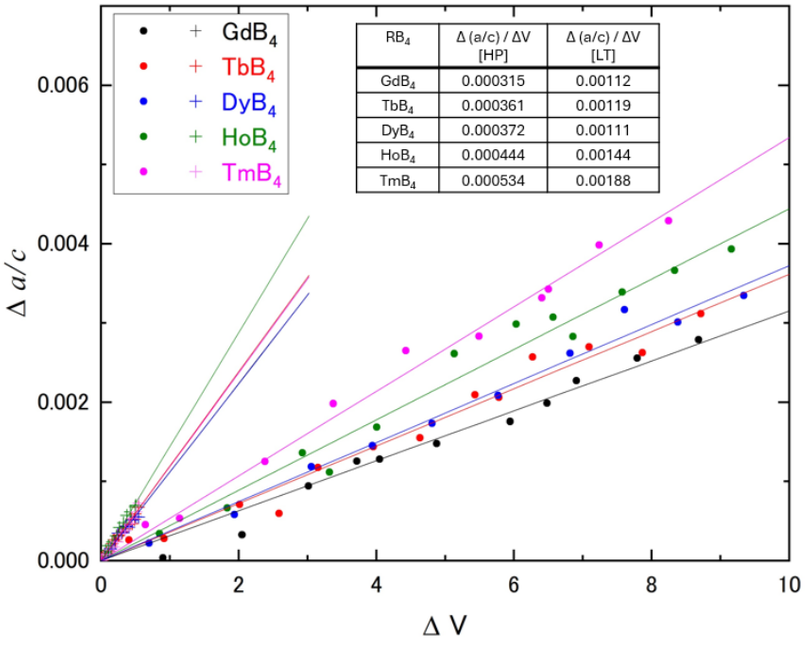

RB_4	Δ (a/c) / ΔV [HP]	Δ (a/c) / ΔV [LT]
GdB_4	0.000315	0.00112
TbB_4	0.000361	0.00119
DyB_4	0.000372	0.00111
HoB_4	0.000444	0.00144
TmB_4	0.000534	0.00188

Figure 7 : Plots of the lattice anisotropy Δ(a/c) per unit volume change. Circles represent changes during compression, while crosses represent changes during cooling. The inset shows a summary table of the axial ratio change per volume change under high pressure or at low temperature.

IV. SUMMARY

High-pressure and low-temperature X-ray diffraction experiments were conducted on RB_4, a tetragonal crystal with SSL, to investigate its structure and lattice parameter changes. The bulk modulus of RB_4, determined from the lattice constants obtained under high pressure, was found to be K_0 = 175–180 GPa, independent of the type of rare-earth atom. When considering the linear compressibility, the *c*-axis was 12%–17% more compressible than the *a*-axis. We consider this anisotropic compression to be related either to the characteristic SSL within the *c*-plane, which impedes compression along the *a*-axis, or to the configuration of *f*-electrons biased toward the *c*-axis.

When comparing the bulk modulus with that of other polyborides, RB_4 lies between RB_6 (approximately 165–168 GPa) and RB_{12} (approximately 206–208 GPa), indicating that the bulk modulus does not simply correlate with boron content, but is instead correlated with the R–B distance of the coordination polyhedron. X-ray

Journal of Applied Physics

AIP Publishing

diffraction patterns at low temperatures down to 90 K indicated that none of the RB_4 compositions underwent structural change. The thermal expansion coefficient was similar to the reported values for isotropic RB_6 along the *c*-axis, but significantly smaller along the *a*-axis. This indicates that even at low temperatures, the *a*/*c* anisotropy increases owing to volume contraction, showing greater anisotropy per unit volume of expansion than compression. This may suggest that magnetic interactions associated with SSL may be involved even at temperatures around 90 K.

SUPPLEMENTARY MATERIALS

See the Supplementary Material for XRD profiles of the present tetraboride samples, and Selected X-ray diffraction patterns of each RB_4 compound under hydrostatic pressure, and their lattice parameters.

ACKNOWLEDGMENTS

The synchrotron radiation experiments were conducted at BL2S1 in AichiSR, AR-NE1 BL18C in Photon Factory (KEK), with the approval of AichiSR (proposal no.2023N1003, 2023N6005, 2024N5004), and KEK (proposal no. 2023G570). This work was supported by JSPS KAKENHI (grant nos. 19H05790 and 23K17711). We are grateful to Y. Umena, and Y. Shibazaki for their help with the XRD experiments at the synchrotron facilities. This work was supported by World Premier International Research Center Initiative (WPI).

AUTHOR DECLARATIONS

Conflict of Interest

The authors have no conflicts to disclose.

Author Contributions

Hitoshi Yusa: Conceptualization (lead); Data curation (lead); Formal analysis (lead); Funding acquisition (lead); Investigation (lead); Methodology (equal); Project administration (lead); Resources (equal); Supervision (lead); Writing – original draft (lead); Writing – review & editing (equal). Fumitoshi Iga: Resources (equal); Methodology (equal); Writing – review & editing (equal).

DATA AVAILABILITY

The data that support the findings of this study are available from the corresponding author upon reasonable request.

REFERENCES

[1] T. Mori, in *Handbook on the Physics and Chemistry of Rare Earths*; *Vol. 38*, edited by K. A. Gschneidner, J.-C. G. Bünzli, and V. K. Pecharsky (Elsevier, 2008), p. 105.

[2] B. Sriram Shastry and B. Sutherland, Physica B+C **108,** 1069 (1981).

[3] F. Iga, A. Shigekawa, Y. Hasegawa, S. Michimura, T. Takabatake, S. Yoshii, T. Yamamoto, M. Hagiwara, and K. Kindo, Journal of Magnetism and Magnetic Materials **310,** e443 (2007).

[4] S. Michimura, A. Shigekawa, F. Iga, M. Sera, T. Takabatake, A. Kikkawa, Y. Tanaka, and K. Katsumata, Journal of Magnetism and Magnetic Materials **310,** e446 (2007).

[5] N. Qureshi, F. Bourdarot, E. Ressouche, W. Knafo, F. Iga, S. Michimura, L. P. Regnault, and F. Duc, Physical Review B **106,** 094427 (2022).

[6] H. Sim, S. Lee, K.-P. Hong, J. Jeong, J. R. Zhang, T. Kamiyama, D. T. Adroja, C. A. Murray, S. P. Thompson, F. Iga, S. Ji, D. Khomskii, and J.-G. Park, Physical Review B **94,** 195128 (2016).

[7] J. A. Blanco, P. J. Brown, A. Stunault, K. Katsumata, F. Iga, and S. Michimura, Physical Review B **73,** 212411 (2006).

[8] J. Fernández-Rodríguez, J. A. Blanco, P. J. Brown, K. Katsumata, A. Kikkawa, F. Iga, and S. Michimura, Physical Review B **72,** 052407 (2005).

[9] S. Gabani, K. Flachbart, K. Siemensmeyer, and T. Mori, Journal of Alloys and Compounds **821,** 153201 (2020).

[10] A. Kikkawa, K. Katsumata, Y. Narumi, K.-i. Suga, T. Fukui, T. Sugaya, K. Kindo, F. Iga, and S. Michimura, Journal of the Physical Society of Japan **76,** 024711 (2007).

[11] S. Yoshii, T. Yamamoto, M. Hagiwara, T. Takeuchi, A. Shigekawa, S. Michimura, F. Iga, T. Takabatake, and K. Kindo, Journal of Magnetism and Magnetic Materials **310,** 1282 (2007).

[12] R. Watanuki, G. Sato, K. Suzuki, M. Ishihara, T. Yanagisawa, Y. Nemoto, and T. Goto, Journal of the Physical Society of Japan **74,** 2169 (2005).

[13] J. Y. Kim, B. K. Cho, and S. H. Han, Journal of Applied Physics **105** (2009).

[14] J. S. Olsen, A. Waśkowska, L. Gerward, G. Vaitheeswaran, V. Kanchana, A. Svane, N. Shitsevalova, and V. B. Fillipov, High Pressure Research **31,** 3 (2011).

[15] E. Deligoz, H. Ozisik, K. Colakoglu, G. Surucu, and Y. O. Ciftci, Journal of Alloys and

Compounds **509,** 1711 (2011).

16 A. S. Panfilov, G. E. Grechnev, I. P. Zhuravleva, A. V. Fedorchenko, and V. B. Muratov, Low Temperature Physics **41,** 193 (2015).

17 C. Pan, S.-Y. Wang, H. Tang, H.-Y. Wu, G.-Y. Shi, K. Cao, H. Jiang, Y.-H. Su, and C. Zhang, Journal of Physics and Chemistry of Solids **164,** 110622 (2022).

18 G. Surucu, H. Ozısık, E. Deligoz, I. R. Shein, A. V. Matovnikov, N. V. Mitroshenkov, A. V. Morozov, and V. V. Novikov, Journal of Alloys and Compounds **862** (2021).

19 V. V. Novikov, N. V. Mitroshenkov, A. V. Matovnikov, D. V. Avdashchenko, S. V. Trubnickov, and A. V. Morozov, Journal of Thermal Analysis and Calorimetry **120,** 1597 (2015).

20 V. V. Novikov, N. V. Mitroshenkov, A. V. Morozov, A. V. Matovnikov, and D. V. Avdashchenko, Journal of Applied Physics **111** (2012).

21 V. V. Novikov and N. V. Mitroshenkov, Physics of the Solid State **54,** 1186 (2012).

22 V. V. Novikov, N. V. Mitroshenkov, A. V. Morozov, A. V. Matovnikov, and D. V. Avdashchenko, Journal of Thermal Analysis and Calorimetry **113,** 779 (2013).

23 F. Iga, N. Shimizu, and T. Takabatake, Journal of Magnetism and Magnetic Materials **177-181,** 337 (1998).

24 T. Tsuchiya, Journal of Geophysical Research: Solid Earth **108,** 002462 (2003).

25 Y. Seto, D. Nishio-Hamane, T. Nagai, and N. Sata, Review of High Pressure Science and Technology **20,** 269 (2010).

26 A. C. Larson and R. B. Von Dreele, Los Alamos National Laboratory Report LAUR**,** 86 (2004).

27 M. G. Pamato, I. G. Wood, D. P. Dobson, S. A. Hunt, and L. Vocadlo, J Appl Crystallogr **51,** 470 (2018).

28 A. Waśkowska, L. Gerward, J. Staun Olsen, K. Ramesh Babu, G. Vaitheeswaran, V. Kanchana, A. Svane, V. B. Filipov, G. Levchenko, and A. Lyaschenko, Acta Materialia **59,** 4886 (2011).

29 D. L. Anderson and O. L. Anderson, Journal of Geophysical Research (1896-1977) **75,** 3494 (1970).

30 H. Yusa, F. Iga, and H. Fujihisa, Inorganic Chemistry (2022).

31 V. V. Novikov, A. V. Morozov, A. V. Matovnikov, D. V. Avdashchenko, Y. N. Polesskaya, N. V. Sakhoshko, B. I. Kornev, V. D. Solomennik, and V. V. Novikova, Physics of the Solid State **53,** 1839 (2011).

32 N. N. Sirota, V. V. Novikov, and A. V. Novikov, Physics of the Solid State **42,** 2093 (2000).